scientific reports

Check for updates

OPEN

Injectable alginate/collagen clindamycin hydrogel for treatment of surgical site infections

Roy K. Park[1,5], Sungwoo Kim[2,5], Jeonghyun An[1], Melissa C. Lee[1], Yunzhi Peter Yang[2,3,4]✉ & Tulio A. Valdez[1]✉

The current standard treatment for surgical site infections (SSIs) is marked by prolonged courses of antibiotics, which have limitations due to antibiotic resistance, systemic side effects, and poor patient adherence. We developed a novel injectable alginate/collagen clindamycin hydrogel that rapidly solidifies upon injection and allows for initial burst release followed by sustained release to maintain therapeutic levels. The rheological, morphological, and in-vitro release kinetics of the hydrogel were characterized. Furthermore, with an in-vivo murine SSI model incubated with logarithmic growth phase 1×10^5 CFU *Staphylococcus aureus*, one time treatment with injectable hydrogel containing 8 mg clindamycin successfully treated SSI comparable to a cumulative systemic antibiotic dose of 42 mg clindamycin. In an implant SSI model, two-time treatment with the injectable clindamycin antibiotic (16 mg total) successfully suppressed infection and prevented recalcitrant infection. To date, no group has developed a clindamycin encapsulated injectable alginate/collagen hydrogel for the treatment of infection. This tunable hydrogel may serve as an effective delivery vehicle for clinical applications in treating SSIs compared to conventionally available treatments.

Keywords Injectable hydrogel, Antibiotic therapy, Imaging, Surgical site infection, Bacterial infection

Surgical site infections (SSI) are the leading cause of hospital readmission following surgical procedures, often resulting in hospital costs exceeding $30,000 USD per admission[1,2]. SSIs involving implants present unique challenges due to increased risks of persistent infection, treatment failure frequently necessitating implant removal, and increased overall mortality[3]. As the population demographic continues to age, national projections have estimated a significant increase in the number of implant surgeries to maintain function in the elderly[4]. This demographic change emphasizes the urgent need for improved SSI management strategies that effectively address both infection control and implant retention.

The current standard of care for SSI treatment involves extended courses of systemic antibiotics, administered either orally or intravenously, depending on the severity and nature of the infection. However, this approach has significant limitations including antibiotic resistance, systemic side effects, and poor patient adherence due to inconvenient dosing schedules[5–7]. As a result, there is a strong clinical need for sustained and localized delivery mechanisms for SSI treatment.

Clindamycin, a lincosamide antibiotic, is frequently prescribed for the treatment of skin and soft tissue infections (SSTIs) for patients with penicillin allergy, including community-acquired methicillin-resistant *Staphylococcus aureus* (CA-MRSA)[10]. However, systemic clindamycin administration is associated with significant risks, such as *Clostridioides difficile* infection, which can cause severe gastrointestinal complications and increased morbidity in the elderly[8,9]. Additionally, clindamycin's time-dependent antibacterial activity necessitates frequent dosing, typically three to four times daily, to maintain effective plasma concentrations[10]. This frequent dosing can be burdensome for patients, leading to poor adherence and reduced treatment efficacy.

Localized delivery systems, such as hydrogels, can address these issues by providing a controlled, sustained release of drug to the infection site. Hydrogels have emerged as widely applicable biomaterials for various biomedical applications, particularly in drug delivery and tissue engineering[11,12]. In the context of infection, the development of a facile, biocompatible hydrogel that not only provides sustained drug release but also resists degradation remains a challenge. Prior studies have developed various antibiotic-loaded hydrogels including

[1]Department of Otolaryngology – Head and Neck Surgery, Stanford University, 801 Welch Rd, Palo Alto, CA 94304, USA. [2]Department of Orthopaedic Surgery, School of Medicine, Stanford University, Stanford, CA 94305, USA. [3]Department of Materials Science and Engineering, School of Engineering, Stanford University, Stanford, CA 94305, USA. [4]Department of Bioengineering, School of Medicine, Stanford University, Stanford, CA 94305, USA. [5]Roy K. Park and Sungwoo Kim contributed equally to this work. ✉email: ypyang@stanford.edu; tvaldez1@stanford.edu

vancomycin, gentamycin, and metronidazole with the use of synthetic polymers[13–16]. Synthetic polymers such as PEG, poly (acrylic acid), and poly(*N*-isopropylacrylamide) in hydrogels can be finely tuned for sustained drug release while maintaining mechanical strength and flexibility[17–19]. However, compared to organic compounds, synthetic polymers may pose the risk of cytotoxicity with prolonged use[19].

Organic compounds, such as alginate and collagen-based hydrogels, have attracted significant attention due to their unique properties and biocompatibility[20]. Alginate, a naturally occurring polysaccharide derived from brown seaweed, forms hydrogels in the presence of divalent cations and offers excellent injectability and biodegradability[21]. When combined with collagen, a major structural protein in the extracellular matrix, these hydrogels can effectively mimic the natural tissue environment, providing both structural support and biological cues[22]. A number of studies have utilized organic compounds to formulate antibiotic hydrogel dressings, but a significant limitation is confinement to superficial skin wounds and inability to be placed into deep wounds in the setting of SSI[23,24].

Recent work has shown that composite hydrogels containing alginate and collagen can create a versatile matrix that can be customized for various drug delivery applications[25]. These hydrogels can be modified in terms of mechanical properties, porosity, and degradation rates, making them particularly suitable for the controlled release of therapeutic agents such as antibiotics[26]. The injectable nature of these hydrogels offers a minimally invasive approach to delivering drugs directly to target sites without the need to re-open the surgical site in the setting of SSIs[27]. Upon injection, the liquid formulation rapidly gels in situ, forming a localized matrix for sustained drug release, offering advantages over systemic delivery[28]. This method ensures high local drug concentrations while minimizing systemic side effects often associated with conventional administration routes[11]. The approach not only improves treatment efficacy but also enhances patient compliance by eliminating the need for frequent dosing and maintaining effective therapeutic concentrations over an extended period. Furthermore, the release kinetics of encapsulated antibiotics, such as clindamycin, can be finely tuned by modifying the hydrogel composition and cross-linking density[25]. This allows for an initial burst release to quickly achieve therapeutic levels, followed by a sustained release to maintain effective drug concentrations over time[29]. The interactions between the drug and the hydrogel matrix, including ionic bonding, hydrogen bonding, and physical entrapment, play crucial roles in modulating the release profile[21]. Understanding these interactions and the resulting release kinetics is essential for optimizing hydrogel formulations and predicting their efficacy in various therapeutic applications[11].

To date, no research group has developed an injectable alginate/collagen-based hydrogel encapsulating clindamycin for targeted delivery to infected regions. In contrast to topical hydrogel dressings, the injectable nature of the hydrogel allows treatment of SSI without need for further invasive surgery to re-open the wound site[17–19]. The organic nature of the alginate/collagen hydrogel also avoids any potential issues with cytotoxicity and has excellent biocompatibility. In this study, we sought to design and evaluate an injectable hydrogel loaded with clindamycin. We assessed the rheological, morphological, and in-vitro release kinetics of the gel. Finally, we examined the in-vivo performance of the clindamycin encapsulated hydrogel in a murine model of SSI, with the aim of achieving precise and sustained local antibiotic release.

Results and discussion

SEM analysis of alginate/collagen hydrogel

The microstructures of collagen and alginate/collagen hydrogels were examined using scanning electron microscopy (SEM) to assess their architectural differences. Freeze-dried hydrogel samples were mounted on stubs and carbon-coated to improve electron conductivity. Figure 1a displays the SEM image of the collagen hydrogel, which reveals a highly porous and fibrous architecture. The collagen fibrils are loosely organized, forming an open network with large, irregular pores. This porous structure is characteristic of the self-assembly of collagen monomers into a weakly crosslinked fibrillar matrix. The observed large pore size suggests improved permeability, potentially facilitating nutrient diffusion. However, this architecture also compromises mechanical stability and structural integrity, rendering the hydrogel more vulnerable to enzymatic degradation. Figure 1b shows the microstructure of the alginate/collagen hydrogel, highlighting a denser and more organized network compared to the pure collagen hydrogel. The fibrillar collagen arrangement is more compact, with finer, well-organized fibers distributed throughout the matrix. The addition of alginate contributes significantly to this enhanced structure by decreasing pore size and increasing hydrogel density. When ionically crosslinked, alginate forms a cohesive network that reinforces the collagen fibrils, resulting in improved stability and reduced porosity. The integration of alginate and collagen is evident from the heterogeneous matrix, where the nanoporous alginate mesh supports and intercalates with the collagen fibrils. This denser, less porous structure likely provides superior mechanical properties and resistance to degradation, making it well-suited for applications requiring stable and durable hydrogels.

The rheological properties of alginate/collagen hydrogels

Figure 1c illustrates the differences in storage modulus (G') between collagen and alginate/collagen hydrogels over a 300-s period. The collagen hydrogel exhibits a relatively low and stable G′, fluctuating between 10 and 17 Pa, indicating a softer, less elastic hydrogel with a looser network structure and fewer crosslinks. This softer structure, as shown in Fig. 1a, makes the collagen hydrogel more susceptible to deformation and less mechanically stable. In contrast, the alginate/collagen hydrogel demonstrates a significant increase in G′, reaching 204 Pa by the end of the 300-s measurement. This rise reflects the formation of a more robust and elastic matrix, enhancing the hydrogel's mechanical stability. The addition of alginate provides additional crosslinking points within the network, contributing to its increased stiffness and elasticity compared to the collagen-only hydrogel. The gradual increase in G' over time can be attributed to ionic crosslinking between alginate and calcium ions, leading to the development of a stronger, more elastic network. Alginate not only enhances G' but also facilitates the gelation

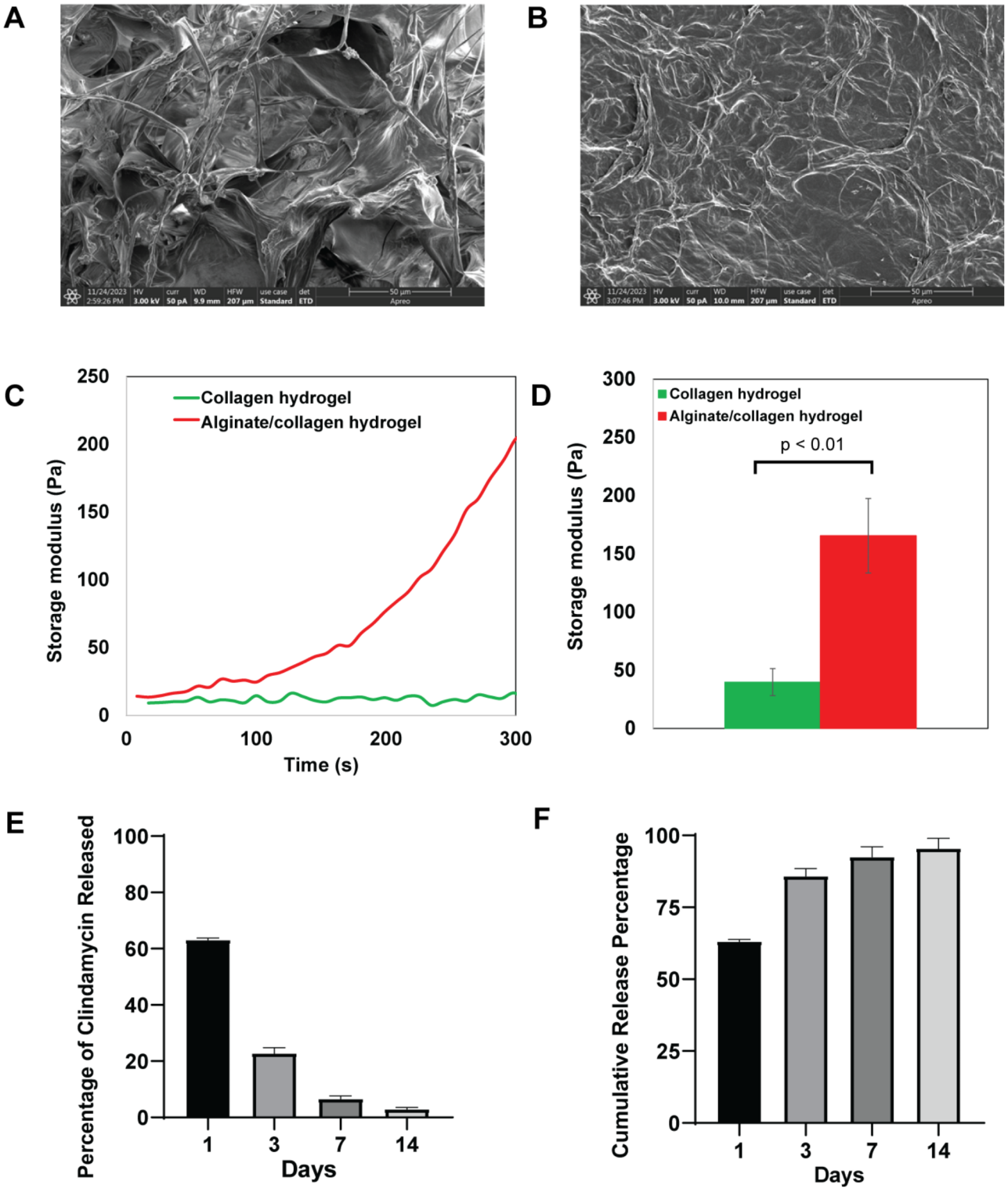

Fig. 1. Characterization of alginate/collagen hydrogels. (**A**, **B**) Scanning electron microscopy (SEM) analysis of (**A**) collagen hydrogel and (**B**) alginate/collagen hydrogel. Magnification of 1000× was utilized to observe micro-scale morphological features of the freeze-dried hydrogels. (**C**) Rheological properties of collagen and alginate/collagen hydrogel were evaluated by storage modulus (G′) of the hydrogels measured over time at 37 °C. (**D**) average storage modulus (G′) of pre-formed hydrogels evaluated after 120 s at 24 °C, reflecting their stabilized mechanical properties. Error bars indicate ± standard deviation (n = 3). (**E**, **F**) In-vitro release kinetics of alginate/collagen hydrogel over a 14 day period. (**E**) Percentage of clindamycin released. (**F**) Overall cumulative percentage released. Error bar represents ± SD (n = 4).

process, resulting in a more rigid and mechanically stable structure. This significant improvement underscores the superior mechanical properties of the alginate/collagen hydrogel relative to collagen alone. The averaged G' of the preformed collagen and alginate/collagen hydrogels was measured after 120 s at 24 °C to evaluate their mechanical properties following complete crosslinking, as shown in Fig. 1d. The collagen hydrogel exhibited a G′ of 40 Pa, whereas the alginate/collagen hydrogel demonstrated a significantly higher G′ of 165 Pa ($p < 0.05$). This result highlights the enhanced stiffness provided by the addition of alginate, likely due to its contribution to the overall crosslinking density within the hydrogel network. The increased crosslinking points introduced by alginate create a more interconnected and robust network, improving both the stiffness and elasticity of the hydrogel.

In-vitro release kinetics of clindamycin

The release kinetics of clindamycin from the alginate/collagen hydrogel were evaluated through an in vitro study over a two-week period. The experiment measured the cumulative release of clindamycin at specific time points, with the data presented in Fig. 1e,f, illustrating both the percentage released at each interval and the overall cumulative release throughout the two-week period. The release profile of clindamycin demonstrated a characteristic pattern, as often observed in hydrogel-based drug delivery systems[11,30]. Initially, there was a substantial burst release, with approximately 63% of the drug being released within the first 24 h. This was followed by a marked decrease in the release rate, with subsequent measurements showing additional releases of 23%, 7%, and 3% at days 3, 7, and 14, respectively. This trend indicates a rapid initial release followed by a more gradual, sustained release that appeared to stabilize after the first week, consistent with the biphasic release patterns in the previous study[31]. Overall, the release of clindamycin from the alginate/collagen hydrogels progressed as follows: 63% by day 1, 86% by day 3, 93% by day 7, and reaching 96% by the end of the two-week period. These results suggest that the hydrogel system was effective in releasing most of the encapsulated clindamycin within the first week, with only a small additional amount released during the second week, aligning with the controlled release characteristics of similar hydrogel systems[29,32].

The observed release pattern can be attributed to the complex interactions between clindamycin and the alginate/collagen hydrogel matrix[12,29]. These interactions likely involve a combination of ionic bonds, hydrogen bonding, and physical entrapment within the hydrogel network. The anionic nature of alginate, due to its carboxylate groups, may form ionic interactions with the protonated amine group of clindamycin under physiological pH conditions[29]. Furthermore, hydrogen bonding between the functional groups of clindamycin and those present in both alginate and collagen could contribute to the drug's retention within the hydrogel matrix[12]. These molecular interactions play a crucial role in modulating the release kinetics of clindamycin[11,30,33,34]. The initial burst release observed may be due to the rapid diffusion of loosely bound drug molecules near the surface of the hydrogel. The subsequent slower release phase likely results from the gradual diffusion of more strongly interacting clindamycin molecules, as well as the slow degradation of the hydrogel matrix itself[31,35]. This biphasic release profile is characteristic of many hydrogel-based drug delivery systems and demonstrates the potential of the alginate/collagen hydrogel for controlled release of clindamycin[11].

Visualizing gel dispersion in-vivo with an ICG encapsulated hydrogel

To evaluate how the performance of the clindamycin encapsulated alginate/collagen hydrogel would change with in-vivo environments, we placed indocyanine green (ICG), an FDA approved fluorophore, into the hydrogel to use fluorescence intensity as a measurement for dispersion (Fig. 2). The ICG encapsulated alginate/collagen hydrogels were then loaded into a clinically relevant surgical site infection (SSI) model. In brief, a small subcutaneous incision was made on the back of the mice, incubated with logarithmic phase bioluminescent

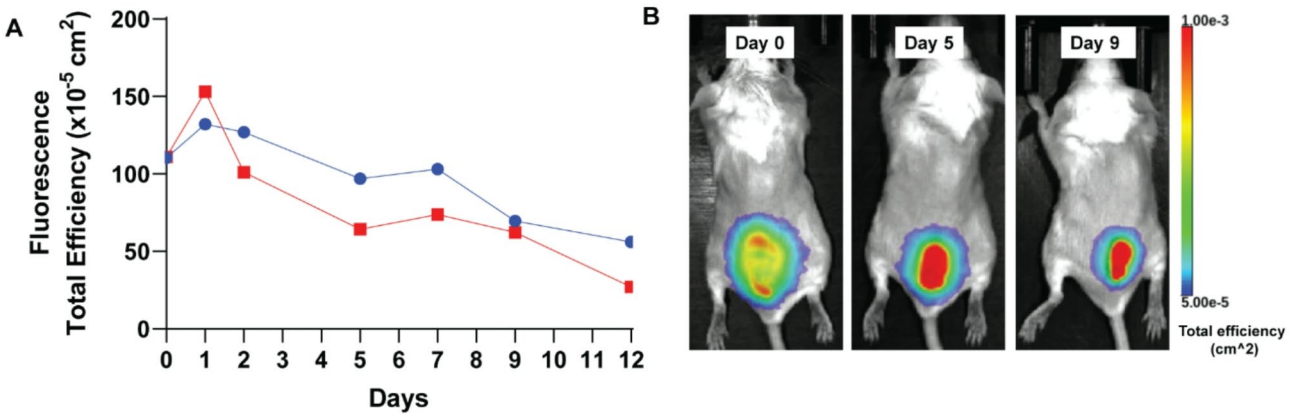

Fig. 2. In-vivo dispersion map of Indocyanine Green (ICG) loaded alginate/collagen hydrogel (**A**) Fluorescence measurements via total efficiency (cm^2) (**B**) Fluorescence intensity changes between days 0, 5, 9 after injection of ICG loaded hydrogel. Each line in A indicates the change of ICG fluorescence intensity in each animal.

Staphylococcus aureus on the wound bed, and allowed to rest for 3 h prior to any treatment to allow for further growth of bacteria.

We then monitored fluorescence intensity via daily imaging with the IVIS (LagoX, Spectral Instruments). Although the premature release of ICG cannot be definitively ruled out, we did not visualize significant dispersion of the fluorescence signal throughout the entire 12 days of monitoring, suggesting that gel stays relatively localized.

Bioluminescence correlation with bacterial load

Prior to employing the clindamycin encapsulated hydrogel for monitoring treatment efficacy, we validated the correlation between bioluminescence signal intensity and bacterial load in our SSI models. We selected *Staphylococcus aureus* Xen36 strain for our models as multiple prior studies have demonstrated robust bioluminescent signals over weeks in murine models[36–38]. To quantify bioluminescence signal, we inoculated the wound bed with active, logarithmic phase *Staphylococcus aureus* (Xen36) at varying concentrations (N = 5 for each group) ranging from 1×10^2 to 1×10^7 CFU. Bioluminescence signal was acquired utilizing an in vivo imaging system (IVIS), which allowed for real-time measurement of bacterial load. We noted a clear increase in bioluminescence signal from 1×10^4 to 1×10^7 CFU, but were unable to detect any bioluminescence signal at bacteria loads lower than 1×10^4 CFU (Fig. 3a). Bioluminescence signal in the 1×10^2 and 1×10^3 CFU groups were similar to non-infected controls, indicating the detection threshold of our system. We then performed a linear regression between the 1×10^4 to 1×10^7 CFU groups, demonstrating a strong correlation coefficient (R^2) at 0.975 (Fig. 3b). This high correlation indicates that bioluminescence intensity is a reliable quantitative measure of bacterial load within this range, providing a robust method for evaluating treatment response in the SSI model.

Efficacy of clindamycin-encapsulated hydrogels in SSI

We first evaluated the efficacy of clindamycin in the treatment of SSI without the presence of an implant. To do so, logarithmic phase bioluminescent *Staphylococcus aureus* was introduced into the infection site, and mice were divided into three groups three hours post-infection: saline control (N = 5), systemic clindamycin phosphate administered three times daily (TID) (N = 5), and a single injection of clindamycin-encapsulated alginate/collagen hydrogel (N = 5) applied directly over the infection site (Fig. 4).

The systemic antibiotic injection was administered at a dose of 100 mg/kg TID subcutaneously for 7 days (equivalent to 42 mg cumulatively for a 20 g mouse) away from the infection site to simulate systemic pharmacokinetics comparable to human dosing[40,41]. The clindamycin encapsulated alginate/collagen hydrogel group received a total dose of 8 mg of clindamycin phosphate in 200 µl of injectable hydrogel overlying the infection site. Contrastingly, the systemic clindamycin treatment group received a cumulative dose of approximately 42 mg over 7 days, indicating the potential dose-sparing benefits of localized hydrogel delivery.

We monitored the degree of infection with daily bioluminescence imaging via the IVIS imaging system (LagoX, Spectral Instruments). The control infection group (saline injection, n = 5) maintained high bioluminescence signal from day 0 (1.9×10^6 photons/s) to day 7 (1.1×10^6 photons/s) indicating active infection. On the other hand, we found that both the one-time hydrogel injection group (n = 5) and systemic clindamycin treatment group (n = 5) showed a rapid and significant reduction in bioluminescence signal starting on day 1 (1.4×10^5 and 7.8×10^4 photons/s respectively) (Fig. 5a,b**).** Bioluminescent signal in the treatment groups remained low to undetectable from day 1 ($p < 0.01$) to the measurement on day 7 ($p < 0.05$), similar to baseline mice

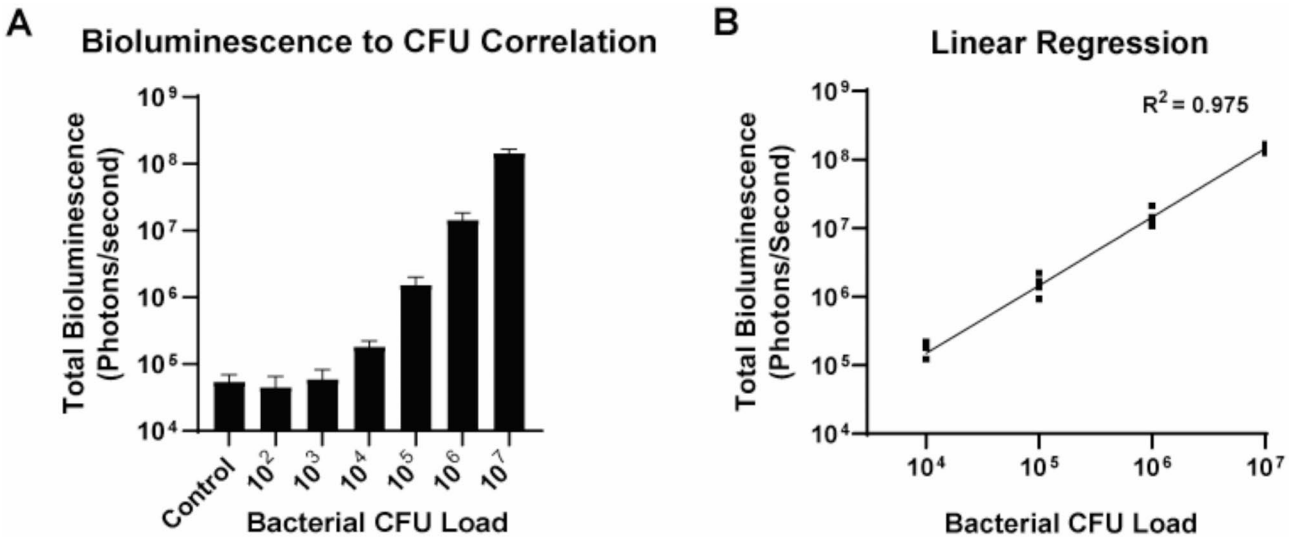

Fig. 3. Bioluminescence to bacterial load (CFU) correlation. (**A**) Total mean bioluminescence signal to bacterial CFU load. (**B**) Linear regression performed for bioluminescence signal from bacteria CFUs 10^4 to 10^7. Error bars represent ± SD (n = 5).

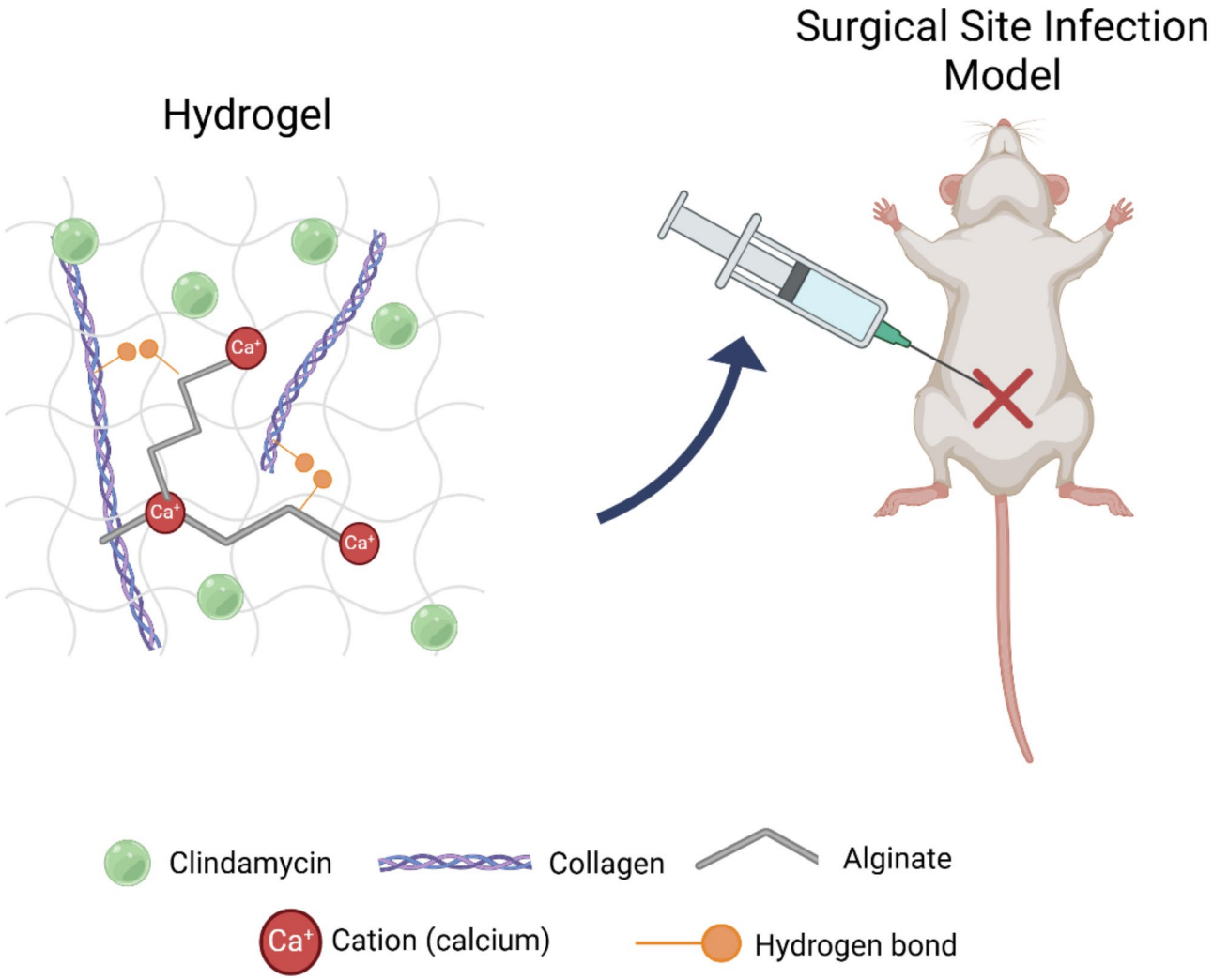

Fig. 4. Experimental schematic of injectable collagen/alginate hydrogel loaded with clindamycin placed into surgical infection site murine model. Created in BioRender.com[39].

without infection suggesting effective infection suppression and likely complete resolution of infection, given the immunocompetent nature of the mice. To further investigate, we assessed an additional treatment group with a sub-therapeutic dose of systemic clindamycin delivered over 7 days, comparable to that of the hydrogel clindamycin group (8 mg). Mice were administered a systemic clindamycin dose of 20 mg/kg TID and monitored daily with bioluminescence (Fig. 5c). This group exhibited a much slower reduction in bioluminescent signal, with bioluminescent signal present on day 7, indicating residual infection and treatment failure. Our findings suggest that one-time targeted treatment with a clindamycin encapsulated alginate/collagen hydrogel can provide sufficient localized therapy to effectively treat SSI at a significantly lower dose compared to conventional systemic treatment. This targeted approach minimizes systemic exposure, improves patient compliance by reducing dosing frequency and leverages the hydrogel's controlled release properties for prolonged therapeutic action directly at the infection site. These results support the potential of clindamycin-encapsulated hydrogels as an effective alternative to conventional systemic antibiotic regimens for localized infection management.

Treatment challenges in implant SSI with single hydrogel administration

Following treatment success of clindamycin-encapsulated hydrogels in treating non-implant SSI, we established a clinically relevant SSI model with a titanium implant. Sterile medical grade titanium wire (0.5 mm diameter) was embedded within the paraspinal muscle of mice and anchored with sutures after incubating the wound with logarithmic growth phase bioluminescent *Staphylococcus aureus* (Xen36). Like the SSI without implant model, mice were divided into the following treatment groups three hours post-infection: saline injection (N = 5), systemic clindamycin phosphate at a dose of 100 mg/kg TID (N = 5), or one time injection of clindamycin (8 mg) hydrogel (N = 5) overlying the infection site.

With daily IVIS imaging over 7 days, we noted high levels of bioluminescence signal in all groups prior to treatment on day 0, indicating active infection prior to treatment (Fig. 6). Compared to the saline control group, the systemic clindamycin treatment group (N = 5) had some residual bioluminescence signal on day 1

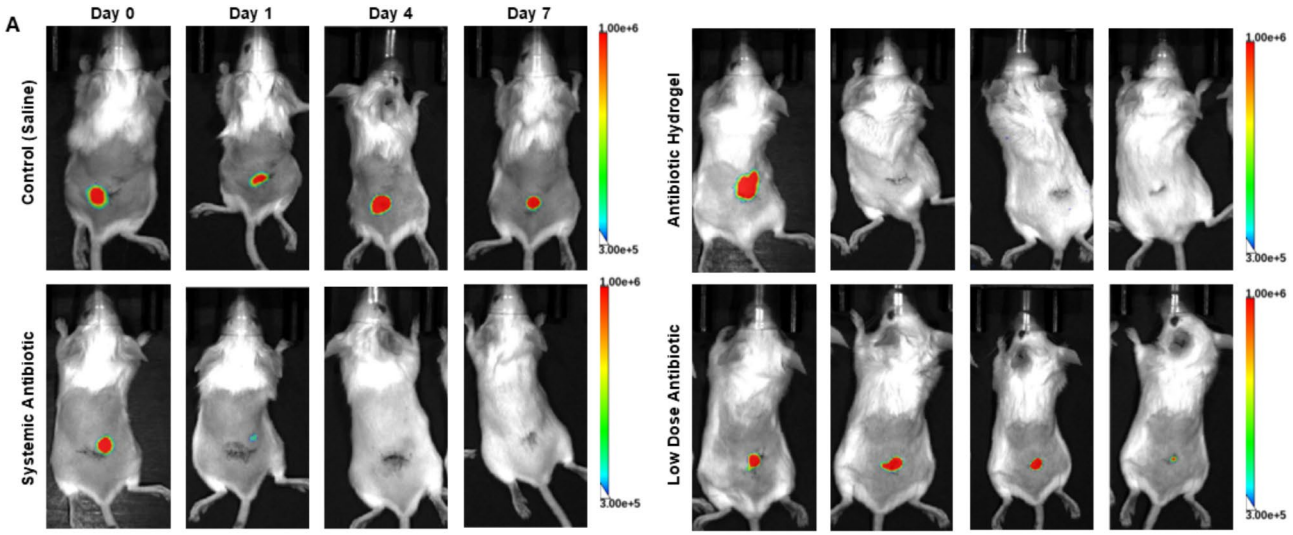

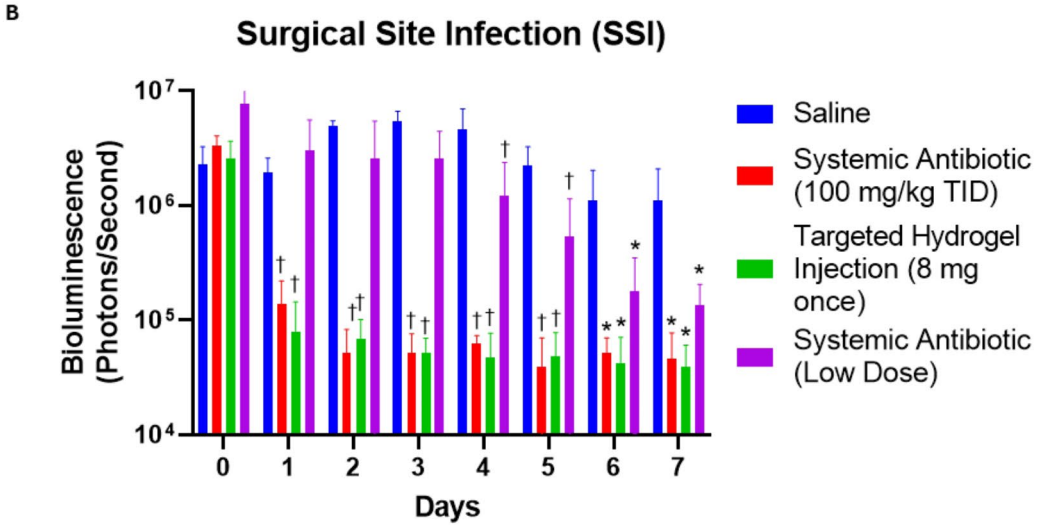

Fig. 5. Treatment of surgical site infection (SSI) with alginate/collagen clindamycin hydrogel (**A**) Bioluminescence signals in mice following treatment with either saline control group (n = 5), systemic antibiotic (n = 5), antibiotic hydrogel (n = 5), or low dose antibiotic (n = 5). (**B**). Total mean bioluminescence changes between saline control group, systemic antibiotic, local hydrogel injection, and low dose antibiotic (20 mg/kg). Mice that received a low dose of systemic antibiotic (20 mg/kg) equivalent to hydrogel injection continued to have infection until the end of treatment. $^{*}p < 0.05$, †$p < 0.01$. Systemic antibiotic, systemic antibiotic (low dose), or targeted hydrogel versus saline group (one-way ANOVA with Tukey tests). Error bars represent ± SD (n = 5).

(1.5×10^5 photons/s, $p < 0.01$), but bioluminescence signal continued to decrease to undetectable levels by day 4 (5×10^4 photons/s, $p < 0.05$), suggesting infection suppression through systemic exposure. Contrastingly, in the one-time injection of clindamycin (8 mg) hydrogel group, bioluminescence signal was undetectable from day 1 ($p < 0.01$) to day 4 ($p < 0.05$) compared to the saline group demonstrating initial infection suppression. However, bioluminescence signal began to rise again from day 5, indicating recurrent infection. These results reflect clinical challenges often encountered in treating implant SSIs, where the implant can act as a nidus for residual infection and biofilm formation, complicating complete bacterial eradication and necessitating prolonged antibiotic courses[42,43].

Recurrent infection in the one-time injection of clindamycin (8 mg) hydrogel group highlights the limitations of one-time localized treatment in the context of implant-associated infections. Implants, especially those made of titanium, are known to support biofilm development and provide a protective environment for bacteria. This makes them much less susceptible to antibiotics[44]. Clinically, implant SSIs often require extended antibiotic therapy due to the increased difficulty in achieving sufficient drug concentrations at the infection site and overcoming biofilm-associated resistance.

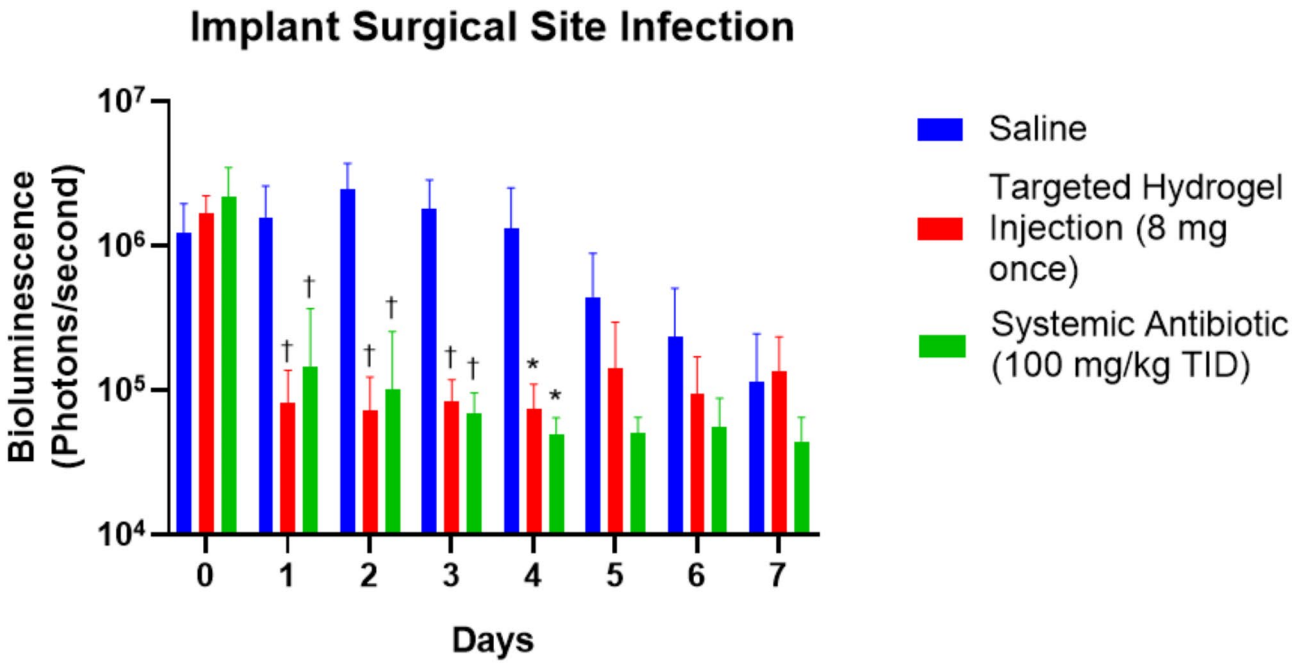

Fig. 6. Bioluminescence signal following treatment of implant surgical site infection (SSI) with systemic antibiotic and targeted injected antibiotic hydrogel. *$p < 0.05$, †$p < 0.01$. Systemic antibiotic or targeted hydrogel versus saline group (one-way ANOVA with Tukey tests). Error bars represent ± SD (n = 5).

Two time injection of antibiotic hydrogel successfully suppresses implant SSI

Given the persistence of infection and treatment failure observed in the one-time clindamycin hydrogel treatment group, we introduced a second dose of the clindamycin hydrogel on day 3 to address potential infection relapse anticipated by day 5 (Fig. 7). To better understand the long-term infection dynamics, we extended infection monitoring using daily IVIS imaging for a total of 10 days. Mice were divided into the following four treatment groups following induction of infection: saline injection (N = 5), systemic clindamycin phosphate at a dose of 100 mg/kg TID for a total of 7 days (N = 5), one time treatment with clindamycin (8 mg) hydrogel (N = 5), or two time injection of clindamycin (8 mg) hydrogel (N = 5) on day 0 and day 3. The systemic antibiotic treatment group did not receive any further doses of antibiotic after day 7.

We noted high bioluminescence signals persisted in the control infection group (saline injection) throughout the 10-day observation period, indicating active infection (Fig. 7a). Compared to the saline control group, the systemic clindamycin treatment group had a sharp decrease in bioluminescence signal from day 1 ($p < 0.05$) to day 7 ($p < 0.01$) comparable to background levels while receiving treatment. However, after treatment was stopped on day 7, one of the mice had recurrence of infection in the following 7 days (on day 10) suggesting residual infection likely due to bacteria and biofilm presence on the implant (Fig. 7b). Similar to the previous experiment, several mice in the one-time clindamycin hydrogel treatment group experienced early infection recurrence within the first week and had sustained bioluminescence signals indicating unresolved infection starting on day 7. On day 10, two of the mice in the one-time clindamycin hydrogel treatment group had detectable levels of bioluminescence indicating infection. In contrast, the cohort with repeat clindamycin hydrogel group treatment on day 3 maintained undetectable bioluminescence levels from day 1 ($p < 0.05$) to day 10 ($p < 0.01$) compared to the control group, indicating successful suppression of the infection. We thus demonstrate that two-time treatment with clindamycin encapsulated alginate/collagen hydrogels had comparable performance to systemic antibiotic treatment and successfully suppresses detectable levels of infection in an implant SSI model. This highlights the potential of a two-time hydrogel approach to serve as a valuable adjunct or alternative to systemic therapy, especially in cases where biofilm-mediated resistance limits treatment success.

The observed undulating pattern of recurrent infection in the one-time hydrogel treatment group can be explained by biofilm formation on the infected implant hardware. Prior studies have demonstrated that very few colony forming units (100 CFUs) in murine models can establish biofilm formation on an implant and lead to recalcitrant, intractable infection[36]. Clinically, retained infected hardware requires aggressive medical therapy with many cases requiring removal of the affected hardware. *Staphylococcus aureus*, in particular, has been associated with greater likelihood of treatment failure when associated with hardware infections[45]. While eradication of biofilm may be unattainable, our findings suggest that two-time injection of the clindamycin encapsulated alginate/collagen hydrogel can effectively suppress infection from becoming active comparable to systemic antibiotics and may be helpful in preventing complete treatment failure. Given its sustained release, local effectiveness, and biocompatibility, this hydrogel-based approach may offer an attractive alternative to conventional antibiotic-loaded beads[46], which are non-biodegradable. Combining localized hydrogel treatment

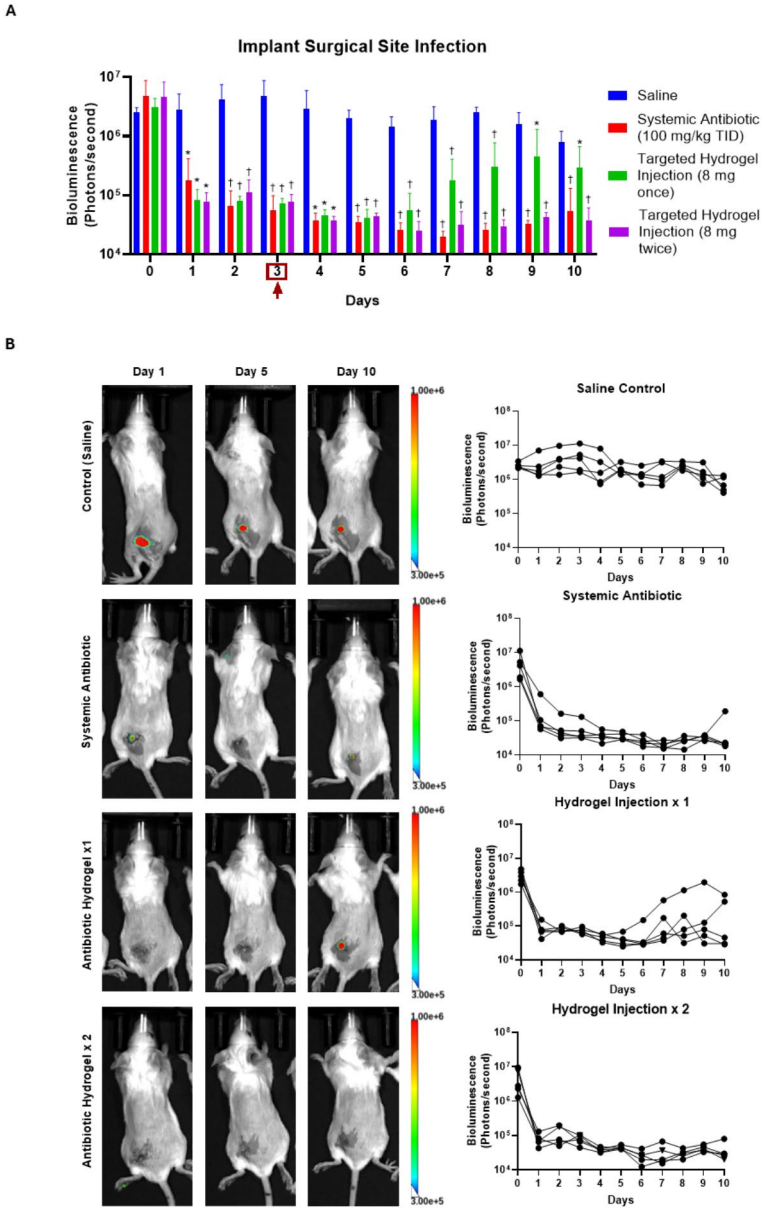

Fig. 7. Treatment of implant surgical site infection (SSI) with bioluminescence monitoring over 10 days (**A**, **B**). Mice were treated with control saline, systemic antibiotic (for 7 days), one-time antibiotic hydrogel injection (day 0), or two time antibiotic hydrogel injection (days 0 and 3). $^{*}p < 0.05$, $\dagger p < 0.01$. Systemic antibiotic, targeted hydrogel injection (one time), or targeted hydrogel injection (twice) versus saline group (one-way ANOVA with Tukey tests). Error bars represent ± SD (n = 5).

with systemic antibiotics could enhance therapeutic outcomes and reduce the need for hardware removal in clinical settings.

Histopathology and immunohistochemistry

Lastly, we assessed overlying infected skin samples using H&E staining following harvest of the overlying skin in the implant models (Fig. 8). When an infection is present, the activation of the immune response leads to subsequent migration of a variety of lymphocytes to combat and phagocytize bacteria[47]. The resultant inflammatory response from infection will lead to vasodilation, fluid leakage, and subsequent edema and fat stranding[47,48]. All these findings can be seen in histopathological sections within immunocompetent animals. In the H&E sections of infected specimens, thickening of the fat layer and abscess were visualized in the control group indicating active infection and a triggered immune response (Fig. 8a). For the treatment groups with systemic antibiotics, there was little to no fat thickening present (Fig. 8b). While the two-time hydrogel injection group (Fig. 8d) also had little to no fat thickening present similar to that of the systemic antibiotic group, there was moderate inflammation present with infiltrates from lymphocytes in the one time hydrogel treatment group (Fig. 8c).

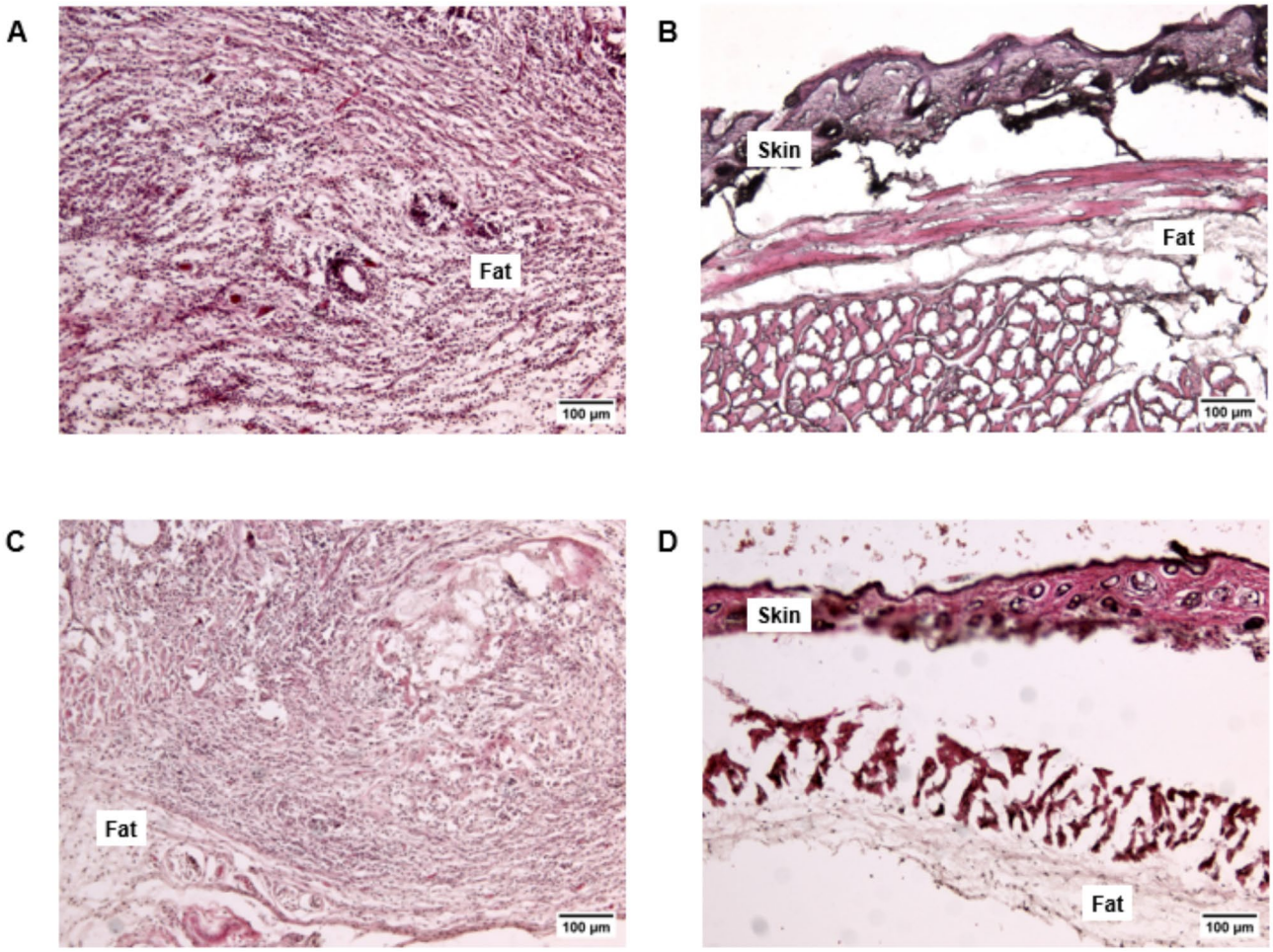

Fig. 8. Histology (H&E) stains of skin samples following treatment. (**A**) Control saline (**B**) Systemic antibiotic treatment (**C**) One time treatment with antibiotic loaded collagen/alginate hydrogel (**D**) Two-time treatment with antibiotic loaded collagen/alginate hydrogel.

Immunohistochemistry (IHC) staining demonstrated an abundance of hematopoietic cells (CD45) and macrophages (F4/80) in the control group (Fig. 9a**).** In mice that received the one time hydrogel injection (Fig. 9c), IHC staining similarly revealed an abundance of hematopoietic cells and macrophages suggesting moderate inflammation and residual infection, consistent with bioluminescence measurements. When comparing the mice that received systemic antibiotic (Fig. 9b) and two-time antibiotic hydrogel injection (Fig. 9d), there were few macrophages and hematopoietic cells present, suggesting only mild inflammation with likely resolution of detectable infection.

This study has several limitations. One limitation is the inability to detect bacterial loads at 1×10^3 CFU and lower with the bioluminescence system. However, we demonstrate that two-time injection of hydrogel provided comparable efficacy to systemic antibiotics, the current clinical gold standard, in suppressing implant SSI. Complete treatment of biofilms remains a challenging issue, with no definitive solutions to date[49]. Injectable clindamycin encapsulated alginate/collagen hydrogels offer a promising option in the limited number of treatments available for SSI, with its minimally invasive nature. Another limitation of the study is the wide variability between different implants and subsequent SSI. Further investigation will be needed to determine if the efficacy of the clindamycin alginate/collagen hydrogel is similar in different infection models such as orthopedic implants.

Conclusion

In this study, we designed and characterized an injectable alginate/collagen hydrogel encapsulated with clindamycin to treat SSIs. The alginate/collagen hydrogel demonstrated a biphasic release kinetic, with burst release followed by a sustained controlled release. Validation testing with murine SSI models demonstrated its ability to successfully treat infection in non-implant infection models. With chronic implant infection models, two-time treatment with the clindamycin encapsulated hydrogel successfully suppressed recalcitrant infection and prevented total treatment failure. Overall, this tunable alginate/collagen hydrogels serves as an effective delivery vehicle for clinical applications in treating SSIs compared to conventionally available treatments.

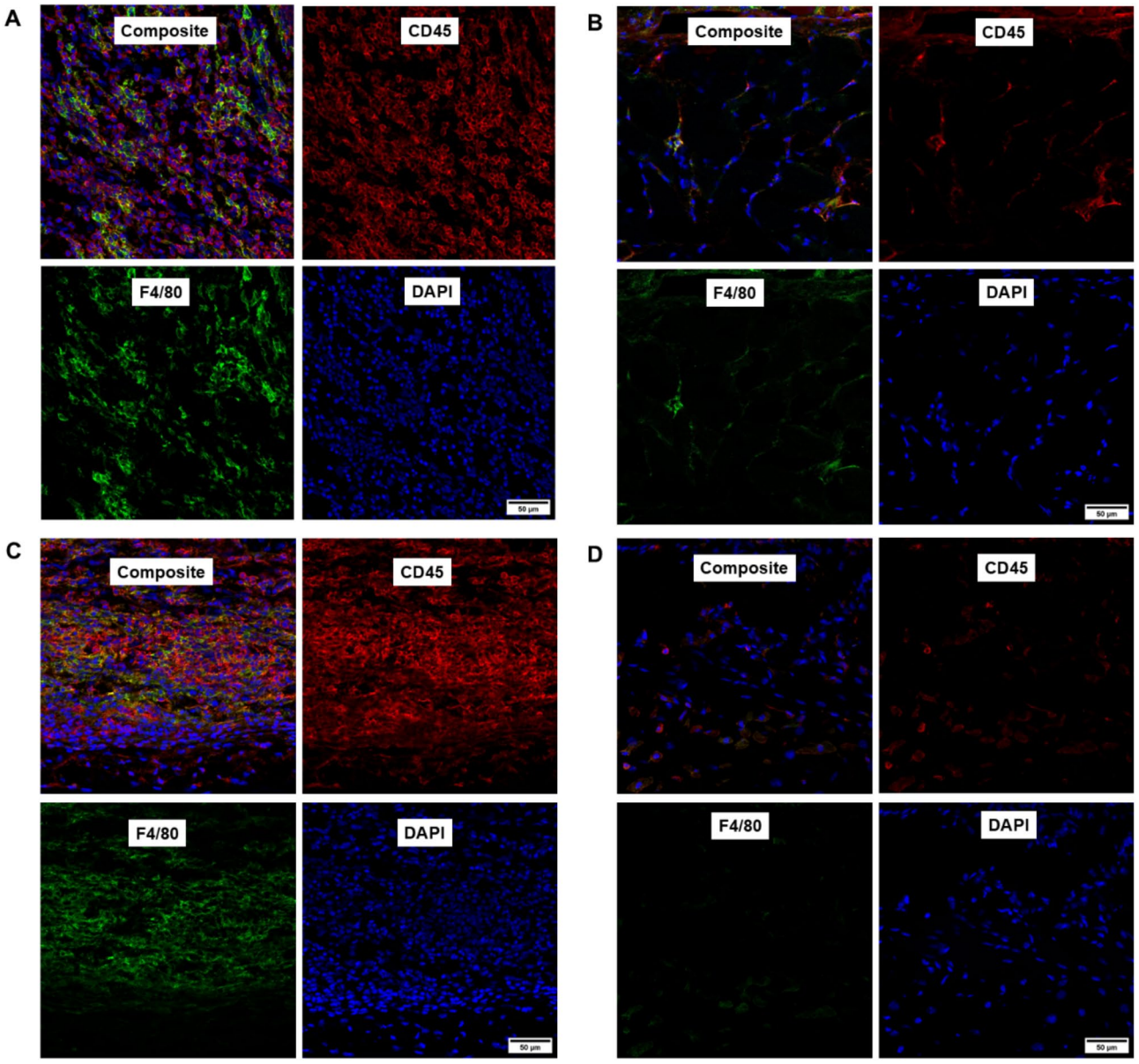

Fig. 9. Immunohistochemistry stains of skin and fat samples following treatment. (**A**) Control saline (**B**) Systemic antibiotic treatment (**C**) One time treatment with antibiotic loaded collagen/alginate hydrogel (**D**) Two-time treatment with antibiotic loaded collagen/alginate hydrogel.

Materials and methods

Materials

Rat tail collagen type I was obtained from Corning Inc. (Corning, NY, USA). Low viscosity sodium alginate (PRONOVA® UP VLVG, 5GM) was procured from NovaMatrix Inc. (Sandvika, Norway). Sodium hydroxide (NaOH), calcium sulfate (CaSO4), 2-(N-Morpholino)ethanesulfonic acid (MES), N-(3-Dimethylaminopropyl)-N-ethylcarbodiimide hydrochloride (EDC), and N-Hydroxysulfosuccinimide (NHS) were acquired from Thermo Fisher Scientific (Waltham, MA, USA). Clindamycin Hydrochloride and Phosphate were acquired from Research Products International (RPI, IL, USA).

Methods

Hydrogel preparation

To create the hydrogel, we first prepared two precursor solutions: sodium alginate and collagen. For the alginate solution, we dissolved low viscosity sodium alginate in calcium-free DMEM at a 2% (w/v) concentration. This solution was then sterilized using 0.22 µm Millex syringe filters, supplemented with sterile 1N NaOH, and stored at 4 °C. The collagen precursor was prepared by first creating a calcium sulfate suspension. We added 1 ml of sterile deionized water to 100 mg of sterile $CaSO_4$ and vortexed for 5 min. We then diluted collagen stock solution (collagen I from rat tail, Corning Inc) with calcium-free DMEM to achieve a 3 mg/ml concentration, working

on ice. This collagen solution was then mixed with the CaSO4 suspension to reach a final $CaSO_4$ concentration of 1.5 mg/ml in the hydrogel solution.

For the antibiotic component, we prepared a clindamycin phosphate solution in PBS at a concentration of 200 mg/ml. We combined 40 µl of this solution with 80 µl of the collagen precursor and mixed thoroughly. To this mixture, we added 80 µl of the alginate precursor (containing 3 µl of 1N NaOH), resulting in a total volume of 200 µl of alginate/collagen hydrogel solution containing 8 mg of clindamycin. Thus, the final hydrogel was formed by combining the collagen and alginate precursor solutions at a 1:1 volume ratio, followed by repeated pipetting to ensure thorough mixing.

Scanning electron microscopy (SEM) The surface morphology of the collagen and alginate/collagen hydrogels was analyzed using a scanning electron microscope (Apreo S LoVac, Thermo Fisher Scientific). Samples were prepared by freezing in liquid nitrogen followed by freeze-drying to maintain structural integrity. The freeze-dried hydrogels were sectioned under liquid nitrogen using a surgical blade. To enhance conductivity and prevent charging, the samples were coated with a 60:40 gold–palladium (Au/Pd) alloy using a sputter coater (SNSF, Stanford, USA). SEM imaging was performed at 3 kV acceleration voltage and 50 pA beam current, with micro-scale features observed at 1,000 × magnification.

Rheological analysis The rheological properties of injectable collagen and alginate/collagen hydrogels were analyzed to assess their mechanical behavior. Hydrogel solutions were loaded onto the Peltier plate of an ARES-G2 rheometer (TA Instruments, New Castle, DE) to monitor the progression of the storage modulus (G′) over time at 37 °C. An 8 mm parallel plate stainless steel geometry with a gap distance of 200 µm was employed. The storage modulus (G′) and loss modulus (G″) were measured using an oscillatory time sweep protocol, with measurements taken from 0 to 300 s to capture the gelation dynamics. Additionally, preformed collagen and alginate/collagen hydrogels were equilibrated on the Peltier plate at 24 °C for 15 min to ensure thermal stability prior to testing. Following equilibration, the storage modulus was recorded after a stabilization period of 120 s at 24 °C. A sinusoidal shear strain of 1% and a frequency of 1 Hz were applied to the hydrogels, and the storage modulus (G') was tracked as a function of time to evaluate their viscoelastic properties.

Release kinetics of clindamycin from alginate/collagen hydrogel in vitro

Clindamycin was encapsulated in an alginate/collagen hydrogel solution as previously described. A volume of 200 µl of the clindamycin-loaded hydrogel solution was injected into the wells of a 24-well plate and incubated at 37 °C for 40 min to allow hydrogel formation. Following this, 1 ml of PBS was added to each well, and the plate was incubated at 37 °C for 14 days. At each time point, the release medium was removed from the wells, replaced with fresh PBS, and transferred to siliconized microcentrifuge tubes for storage in a − 20 °C freezer. Once all release media were collected, clindamycin content was measured using a NanoDrop™ One/OneC Microvolume UV–Vis Spectrophotometer at 210 nm (Thermo Scientific™), following the manufacturer's instructions.

Preparation of bioluminescent Staphylococcus aureus for in-vivo models

Bioluminescent *Staphylococcus aureus* (Xen36, Perkin Elmer) was first plated onto a selective mannitol salt agar plate. Following this, a single colony was grown overnight in Tryptic Soy Broth (TSB) at 37 °C. 100 µl of overnight culture was then placed into 10 ml of fresh TSB and grown until logarithmic phase at $OD_{600} = 0.4$ (TECAN Plate Reader). Bacteria were then centrifuged, washed with PBS × 3, and suspended to a concentration of 1×10^7 CFU/ml to use as inoculum for the infection models. The in-vitro minimum inhibitory concentration (MIC) with clindamycin of the *Staphylococcus aureus* (Xen36) strain used was ≤ 0.5 µg/mL as determined by an independent clinical laboratory (VHA Public Health Reference Laboratory, Veterans Affairs Palo Health Care System).

Murine surgical site infection models (subcutaneous and implant Infection)

All procedures were approved by the Stanford Administrative Panel on Biosafety (APB) and the Stanford Administrative Panel on Laboratory Animal Care (APLAC), and all procedures were performed in accordance with the Stanford Administrative Panel on Biosafety (APB) and the Stanford Administrative Panel on Laboratory Animal Care (APLAC). All experimental procedures complied with ARRIVE guidelines. Following the final experiment, all mice were euthanized in accordance with American Veterinary Medical Association (AVMA) guidelines with carbon dioxide in a gas chamber provided by the Stanford animal research facility.

For the subcutaneous surgical site infection (SSI) model, 6–8 week old balb/c female mice (Jackson Laboratory) around 20 g were anesthetized with 2% v/v isoflurane. Following this, a 2 cm incision was made on the back of the mice and 1×10^5 CFU of bioluminescent logarithmic phase *Staphylococcus aureus* (Xen36, Perkin Elmer) was placed into the subcutaneous pocket. The incision was closed with 5–0 Prolene in an interrupted fashion and sealed with Vetbond (3M).

Similarly, we created a surgical site implant infection model with titanium wire. 6–8 week balb/c female mice were first anesthetized by 2% v/v isoflurane. Following this, an incision was made on the back of the mice and underlying left paraspinal muscles at the level of lower back were identified. A cut on the paraspinal muscles was then made, and sterile medical grade pure titanium wire (0.5 mm diameter, standardized to 7 mm length) was implanted within the muscle. 1×10^5 CFU of bioluminescent logarithmic phase *Staphylococcus aureus* then placed into the wound overlying the implant and the implant was anchored with 4–0 Vicryls in an interrupted fashion. Care was taken to ensure that the titanium implants were embedded within the muscle at the same level and fashion for every animal to ensure consistency. The superficial skin wound was then closed with 5–0 Prolene in an interrupted fashion and sealed with Vetbond (3M). All mice were administered Ethiqa XR (Buprenorphine ER) and meloxicam for appropriate pain control.

Quantification of bioluminescence signal
All bioluminescence imaging was performed with LagoX, an IVIS imager with a CCD camera cooled to − 90 °C (Spectral Instruments Imaging). Images were acquired with low binning and exposure time up to 180 s (3 min). Bioluminescence signals were quantified with Aura Software (Spectral Instruments Imaging) via averaged total emission radiance units (photons/second).

Visualization of gel dispersion with indocyanine green (ICG)
To determine in-vivo gel dispersion, clindamycin encapsulated alginate/collagen hydrogels were supplemented with indocyanine green (ICG) at 100 µM. Alginate/collagen hydrogels encapsulated with ICG were placed into the infected region of the SSI model (N = 2) as previously described and serially followed via fluorescence imaging for up to 12 days. Fluorescence imaging was performed with the IVIS imager, LagoX (Spectral Instruments Imaging). Settings were set at the following: medium binning, up to 30 s exposure, excitation at 770 nm, and emission filter at 810 nm. Fluorescence signals were quantified with Aura Software (Spectral instruments) as total efficiency (cm^2).

Treatment of SSI with clindamycin encapsulated alginate/collagen hydrogel
Subcutaneous and implant murine SSI models were created as previously described. 3 h following incubation of logarithmic phase growth bacteria, mice were anesthetized by 2% v/v isoflurane. Following this, 200 µl of the clindamycin (8 mg) encapsulated alginate/collagen hydrogel was injected via a 28-gauge needle over the infection site. Mice treated with systemic antibiotic (clindamycin phosphate in sterile water) were treated with 100 mg/kg TID (three times daily) dosing via subcutaneous injection far away from the infection site over 7 days. Similarly, the saline (no antibiotic control) group received 50 µl TID injections of saline over 7 days.

Histopathology
Mice skin overlying the infected region was harvested after euthanasia and placed in 4% paraformaldehyde (Thermofisher) for 24 h at 4 C. Specimens were then placed in 30% (w/v) sucrose solution (Thermofisher) for 24 h at 4 C and placed in OCT (Tissue-Tek) solution mixture ratios 70:30, 50:50, 30:70, 10:90, and 0:100 respectively. Cryosectioning was performed at 10 um thickness and hematoxylin and eosin (H&E) staining performed. Slides were imaged with a Leica DM2000 LED microscope at 10× objective magnification with an Allied Vision U-1240c color camera. Immunohistochemistry staining was performed with F4/80 monoclonal antibody (Invitrogen) for macrophage staining and CD45 antibody (R&D Systems) for hematopoietic cell staining. Secondary antibody staining was performed with Alexa Fluor Plus 488 (ThermoFisher) and Alexa Fluor 633 (ThermoFisher) respectively. Confocal images were obtained with the Zeiss LSM 700 under 20× objective magnification and arranged on ImageJ.

Statistical analysis
Data was analyzed via a one-way ANOVA with Tukey tests for comparison on GraphPad Prism 8.0. For statistical analysis comparing rheological properties of collagen and alginate/collagen hydrogels, a two-sided t-test was performed. Data was considered statistically significant when p values were less than 0.05.

Data availability
Data and materials in this study are available upon reasonable request to the corresponding authors.

Received: 10 December 2024; Accepted: 26 February 2025
Published online: 07 March 2025

References
1. Shah, R. et al. Evaluation of readmissions due to surgical site infections: A potential target for quality improvement. *Am. J. Surg.* **214**, 773–779. https://doi.org/10.1016/j.amjsurg.2017.04.011 (2017).
2. Urban, J. A. Cost analysis of surgical site infections. *Surg. Infect. (Larchmt)* **7**(Suppl 1), S19-22. https://doi.org/10.1089/sur.2006.7.s1-19 (2006).
3. Agarwal, A. et al. Implant retention or removal for management of surgical site infection after spinal surgery. *Global Spine J.* **10**, 640–646. https://doi.org/10.1177/2192568219869330 (2020).
4. Shichman, I. et al. Projections and epidemiology of primary hip and knee arthroplasty in medicare patients to 2040–2060. *JB JS Open Access* https://doi.org/10.2106/JBJS.OA.22.00112 (2023).
5. Dohmen, P. M. Antibiotic resistance in common pathogens reinforces the need to minimise surgical site infections. *J. Hosp. Infect.* **70**(Suppl 2), 15–20. https://doi.org/10.1016/S0195-6701(08)60019-5 (2008).
6. Llor, C. & Bjerrum, L. Antimicrobial resistance: risk associated with antibiotic overuse and initiatives to reduce the problem. *Ther. Adv. Drug Saf.* **5**, 229–241. https://doi.org/10.1177/2042098614554919 (2014).
7. Fernandes, M. et al. Non-adherence to antibiotic therapy in patients visiting community pharmacies. *Int. J. Clin. Pharm.* **36**, 86–91. https://doi.org/10.1007/s11096-013-9850-4 (2014).
8. Duffy, C. R. et al. Clindamycin, gentamicin, and risk of *Clostridium difficile* infection and acute kidney injury during delivery hospitalizations. *Obstet. Gynecol.* **135**, 59–67. https://doi.org/10.1097/AOG.0000000000003568 (2020).
9. Climo, M. W. et al. Hospital-wide restriction of clindamycin: effect on the incidence of *Clostridium difficile*-associated diarrhea and cost. *Ann. Intern. Med.* **128**, 989–995. https://doi.org/10.7326/0003-4819-128-12_part_1-199806150-00005 (1998).
10. Murphy, P. B., Bistas, K. G., Patel, P. & Le, J. K. in *StatPearls* (2024).
11. Hoare, T. R. & Kohane, D. S. Hydrogels in drug delivery: Progress and challenges. *Polymer* **49**, 1993–2007. https://doi.org/10.1016/j.polymer.2008.01.027 (2008).
12. Lee, K. Y. & Mooney, D. J. Alginate: Properties and biomedical applications. *Prog. Polym. Sci.* **37**, 106–126. https://doi.org/10.1016/j.progpolymsci.2011.06.003 (2012).
13. Florczyk, A., Krajcer, A., Wojcik, K. & Lewandowska-Lancucka, J. Innovative vancomycin-loaded hydrogel-based systems - New opportunities for the antibiotic therapy. *Int. J. Nanomed.* **19**, 3991–4005. https://doi.org/10.2147/IJN.S443051 (2024).

14. Zubik, K., Singhsa, P., Wang, Y., Manuspiya, H. & Narain, R. Thermo-responsive poly(N-isopropylacrylamide)-cellulose nanocrystals hybrid hydrogels for wound dressing. *Polymers* **9**, 119. https://doi.org/10.3390/polym9040119 (2017).
15. Jeong, J. O. et al. Preparation of radiation cross-linked poly(acrylic acid) hydrogel containing metronidazole with enhanced antibacterial activity. *Int. J. Mol. Sci.* **21**, 187. https://doi.org/10.3390/ijms21010187 (2019).
16. Jiang, F. et al. A multifunctional hydrogel dressing loaded with antibiotics for healing of infected wound. *Int. J. Pharm.* **666**, 124770. https://doi.org/10.1016/j.ijpharm.2024.124770 (2024).
17. Sun, S. et al. Vancomycin-loaded in situ gelled hydrogel as an antibacterial system for enhancing repair of infected bone defects. *Int. J. Nanomed.* **19**, 10227–10245. https://doi.org/10.2147/IJN.S448876 (2024).
18. Boot, W. et al. An antibiotic-loaded hydrogel demonstrates efficacy as prophylaxis and treatment in a large animal model of orthopaedic device-related infection. *Front. Cell Infect. Microbiol.* **12**, 826392. https://doi.org/10.3389/fcimb.2022.826392 (2022).
19. Bashir, S. et al. Fundamental concepts of hydrogels: Synthesis, properties, and their applications. *Polymers (Basel)* **12**, 2702. https://doi.org/10.3390/polym12112702 (2020).
20. Mantha, S. et al. Smart hydrogels in tissue engineering and regenerative medicine. *Materials (Basel)* **12**, 3323. https://doi.org/10.3390/ma12203323 (2019).
21. Augst, A. D., Kong, H. J. & Mooney, D. J. Alginate hydrogels as biomaterials. *Macromol. Biosci.* **6**, 623–633. https://doi.org/10.1002/mabi.200600069 (2006).
22. Drury, J. L. & Mooney, D. J. Hydrogels for tissue engineering: Scaffold design variables and applications. *Biomaterials* **24**, 4337–4351. https://doi.org/10.1016/s0142-9612(03)00340-5 (2003).
23. Shi, S. et al. Sustained release of alginate hydrogel containing antimicrobial peptide Chol-37(F34-R) in vitro and its effect on wound healing in murine model of *Pseudomonas aeruginosa* infection. *J. Vet. Sci.* **24**, e44. https://doi.org/10.4142/jvs.22319 (2023).
24. Jarman, E. et al. Human-Derived collagen hydrogel as an antibiotic vehicle for topical treatment of bacterial biofilms. *PLoS One* **19**, e0303039. https://doi.org/10.1371/journal.pone.0303039 (2024).
25. Li, J. & Mooney, D. J. Designing hydrogels for controlled drug delivery. *Nat. Rev. Mater.* https://doi.org/10.1038/natrevmats.2016.71 (2016).
26. Li, Z., Ramay, H. R., Hauch, K. D., Xiao, D. & Zhang, M. Chitosan-alginate hybrid scaffolds for bone tissue engineering. *Biomaterials* **26**, 3919–3928. https://doi.org/10.1016/j.biomaterials.2004.09.062 (2005).
27. Antoine, E. E., Vlachos, P. P. & Rylander, M. N. Tunable collagen I hydrogels for engineered physiological tissue micro-environments. *PLoS One* **10**, e0122500. https://doi.org/10.1371/journal.pone.0122500 (2015).
28. Kong, H. J., Lee, K. Y. & Mooney, D. J. Decoupling the dependence of rheological/mechanical properties of hydrogels from solids concentration. *Polymer* **43**, 6239–6246 (2002).
29. Rinaudo, M. Main properties and current applications of some polysaccharides as biomaterials. *Polym. Int.* **57**, 397–430 (2008).
30. Siepmann, J. & Gopferich, A. Mathematical modeling of bioerodible, polymeric drug delivery systems. *Adv. Drug Deliv. Rev.* **48**, 229–247. https://doi.org/10.1016/s0169-409x(01)00116-8 (2001).
31. Qiu, Y. & Park, K. Environment-sensitive hydrogels for drug delivery. *Adv. Drug Deliv. Rev.* **53**, 321–339. https://doi.org/10.1016/s0169-409x(01)00203-4 (2001).
32. Tomic, S. L. et al. Alginate-based hydrogels and Scaffolds for biomedical applications. *Mar. Drugs* **21**, 177. https://doi.org/10.3390/md21030177 (2023).
33. Narayanaswamy, R. & Torchilin, V. P. Hydrogels and their applications in targeted drug delivery. *Molecules* **24**, 603. https://doi.org/10.3390/molecules24030603 (2019).
34. Mukherjee, K. et al. Alginate based semi-IPN and IPN hydrogel for drug delivery and regenerative medicine. *J. Drug Deliv. Sci. Technol.* **92**, 105402 (2024).
35. Bouhadir, K. H. et al. Degradation of partially oxidized alginate and its potential application for tissue engineering. *Biotechnol. Prog.* **17**, 945–950. https://doi.org/10.1021/bp010070p (2001).
36. Pribaz, J. R. et al. Mouse model of chronic post-arthroplasty infection: Noninvasive in vivo bioluminescence imaging to monitor bacterial burden for long-term study. *J. Orthop. Res.* **30**, 335–340. https://doi.org/10.1002/jor.21519 (2012).
37. Hu, Y. et al. Combinatory antibiotic therapy increases rate of bacterial kill but not final outcome in a novel mouse model of Staphylococcus aureus spinal implant infection. *PLoS One* **12**, e0173019. https://doi.org/10.1371/journal.pone.0173019 (2017).
38. Kelley, B. V. et al. In vivo mouse model of spinal implant infection. *J. Vis. Exp.* https://doi.org/10.3791/60560 (2020).
39. Created in BioRender. P, R. https://BioRender.com/a08p592(2025).
40. Guo, Y. et al. In vivo bioluminescence imaging to evaluate systemic and topical antibiotics against community-acquired methicillin-resistant Staphylococcus aureus-infected skin wounds in mice. *Antimicrob. Agents Chemother.* **57**, 855–863. https://doi.org/10.1128/AAC.01003-12 (2013).
41. Azeh, I. et al. Protein synthesis inhibiting clindamycin improves outcome in a mouse model of *Staphylococcus aureus* sepsis compared with the cell wall active ceftriaxone. *Crit. Care Med.* **30**, 1560–1564. https://doi.org/10.1097/00003246-200207000-00027 (2002).
42. Veerachamy, S., Yarlagadda, T., Manivasagam, G. & Yarlagadda, P. K. Bacterial adherence and biofilm formation on medical implants: a review. *Proc. Inst. Mech. Eng. H* **228**, 1083–1099. https://doi.org/10.1177/0954411914556137 (2014).
43. Rao, N., Crossett, L. S., Sinha, R. K. & Le Frock, J. L. Long-term suppression of infection in total joint arthroplasty. *Clin. Orthop. Relat. Res.* **414**, 55–60. https://doi.org/10.1097/01.blo.0000087321.60612.cf (2003).
44. Zhao, L., Chu, P. K., Zhang, Y. & Wu, Z. Antibacterial coatings on titanium implants. *J. Biomed. Mater. Res. B Appl. Biomater.* **91**, 470–480. https://doi.org/10.1002/jbm.b.31463 (2009).
45. Espindola, R. et al. Rates and predictors of treatment failure in *Staphylococcus aureus* prosthetic joint infections according to different management strategies: A multinational cohort study-The ARTHR-IS Study Group. *Infect. Dis. Ther.* **11**, 2177–2203. https://doi.org/10.1007/s40121-022-00701-0 (2022).
46. Bistolfi, A. et al. Antibiotic-loaded cement in orthopedic surgery: A review. *ISRN Orthop.* **2011**, 290851. https://doi.org/10.5402/2011/290851 (2011).
47. Rock, K. L., Latz, E., Ontiveros, F. & Kono, H. The sterile inflammatory response. *Annu. Rev. Immunol.* **28**, 321–342. https://doi.org/10.1146/annurev-immunol-030409-101311 (2010).
48. Wiig, H. Pathophysiology of tissue fluid accumulation in inflammation. *J. Physiol.* **589**, 2945–2953. https://doi.org/10.1113/jphysiol.2011.206136 (2011).
49. Verderosa, A. D., Totsika, M. & Fairfull-Smith, K. E. Bacterial biofilm eradication agents: A current review. *Front. Chem.* **7**, 824. https://doi.org/10.3389/fchem.2019.00824 (2019).

Acknowledgements

This research was partially funded through the financial support of NIAMS grants R01AR072613 (YPY), R01AR074458 (YPY), DoD grants W81XWH-20-1-0343 (YPY), and W81XWH-21-PR211291 (YPY). We also acknowledge the support of the Stanford Clinician Scientist Training Program, 5R25DC020174 (RKP).

Author contributions

RKP, SK, YPY, and TAV conceived the original idea. RKP, SK, and JA performed all experiments. RKP, SK, and

MCL drafted the manuscript with contributions from all authors. YPY and TAV supervised the research. RKP and TAV are responsible for all data.

Declarations

Competing interests
The authors declare no competing interests.

Additional information
Correspondence and requests for materials should be addressed to Y.P.Y. or T.A.V.

Reprints and permissions information is available at www.nature.com/reprints.

Publisher's note Springer Nature remains neutral with regard to jurisdictional claims in published maps and institutional affiliations.